Drug Derived Fluorescent Probes for the Specific Visualization of Cannabinoid Type 2 Receptor - A Toolbox Approach

Thais Gazzi,[a] Benjamin Brennecke,[a] Kenneth Atz,[b] Claudia Korn,[b] David Sykes,[c] Roman C. Sarott,[d] Matthias V. Westphal,[d] Patrick Pfaff,[d] Marie Weise,[a] Yelena Mostinski,[a] Bradley L. Hoare,[c] Tamara Miljuš,[c] Maira Mexi,[c] Wolfgang Guba,[b] André Alker,[b] Arne C. Rufer,[b] Eric A. Kusznir,[b] Sylwia Huber,[b] Catarina Raposo,[b] Elisabeth A. Zirwes,[b] Anja Osterwald,[b] Anto Pavlovic,[b] Svenja Moes,[b] Jennifer Beck,[b] Irene Benito-Cuesta,[e] Teresa Grande,[e] Faye Drawnel,[b] Gabriella Widmer,[b] Daniela Holzer,[b] Tom van der Wel,[f] Harpreet Mandhair,[g] Yurii Saroz,[h] Natasha Grimsey,[h] Michael Honer,[b] Jürgen Fingerle,[b] Klaus Gawrisch,[i] Julián Romero,[e] Cecilia J. Hillard,[j] Peter J. McCormick,[k] Zoltan V. Varga,[i,l] Mario van der Stelt,[f] Pal Pacher,[i] Jürg Gertsch,[g] Christoph Ullmer,[b] Sergio Oddi,[m,n] Mauro Maccarrone,[n,o] Dmitry B. Veprintsev,[c] Erick M. Carreira,[d] Uwe Grether,*[b] and Marc Nazaré*[a]

Abstract: Cannabinoid type 2 receptor (CB_2R) is a fundamental part of the endocannabinoid signaling system (eCB system), and is known to play an important role in tissue injury, inflammation, cancer and pain. In stark contrast to its significance, the underlying signaling mechanisms and tissue expression profiles are poorly understood. Due to its low expression in healthy tissue and lack of reliable chemical tools, CB_2R visualization in live cells remains uncharted. Here we report the development of a drug derived toolbox of highly potent, CB_2R-selective fluorescent probes based on reverse design. Extensive validation in several applications such as CB_2R detection in flow cytometry and time-resolved imaging, and the development of a novel fluorescent-based TR-FRET assay to generate kinetic and equilibrium binding data demonstrate the high versatility of our toolbox. These probes are the first to preserve affinity and efficacy in both human and mouse CB_2R, a crucial aspect for preclinical translatability, and to enable imaging of CB2R internalization in living cells using confocal microscopy.

[a] Thais Gazzi, Benjamin Brennecke, Marie Weise, Dr. Yelena Mostinski, Dr. Marc Nazaré
Leibniz-Institut für Molekulare Pharmakologie FMP
Campus Berlin-Buch, 13125 Berlin, Germany
E-mail: nazare@fmp-berlin.de

[b] Dr. Claudia Korn, Dr. Wolfgang Guba, André Alker, Dr. Arne C. Rufer, Eric Kusznir, Dr. Sylwia Huber, Dr. Catarina Raposo, Elisabeth A. Zirwes, Anja Osterwald, Anto Pavlovic, Svenja Moes, Jennifer Beck, Dr. Faye Drawnel, Gabriella Widmer, Daniela Holzer, Dr. Michael Honer, Dr. Jürgen Fingerle, Dr. Christoph Ullmer, Dr. Uwe Grether
Roche Pharma Research & Early Development, Roche Innovation Center Basel, F. Hoffmann-La Roche Ltd., 4070 Basel, Switzerland
E-Mail: uwe.grether@roche.com

[c] Dr. David Sykes, Bradley L. Hoare, Dr. Tamara Miljuš, Maira Mexi, Prof. Dr. Dmitry B. Veprintsev
Faculty of Medicine & Health Sciences, University of Nottingham, Nottingham NG7 2UH, England; United Centre of Membrane Proteins and Receptors (COMPARE), University of Birmingham and University of Nottingham, Midlands, England

[d] Roman C. Sarott, Dr. Matthias V. Westphal, Patrick Pfaff, Prof. Dr. Erick M. Carreira
Laboratorium für Organische Chemie, Eidgenössische Technische Hochschule Zürich, Vladimir-Prelog-Weg 3, 8093 Zürich, Switzerland

[e] Dr. Irene Benito-Cuesta, Dr. Teresa Grande, Prof. Dr. Julián Romero
Faculty of Experimental Sciences, Universidad Francisco de Vitoria, Pozuelo de Alarcón, 28223, Madrid, Spain

[f] Dr. Tom van der Wel, Prof. Dr. Mario van der Stelt
Department of Molecular Physiology, Leiden Institute of Chemistry,

[g] Harpreet Mandhair, Prof. Dr. Jürg Gertsch
Institute of Biochemistry and Molecular Medicine, University of Bern, 3012 Bern, Switzerland

[h] Yurii Saroz, Dr. Natasha Grimsey
Department of Pharmacology and Clinical Pharmacology, School of Medical Sciences, Faculty of Medical and Health Sciences, University of Auckland, 1142 Auckland, New Zealand

[i] Dr. Klaus Gawrisch, Dr. Zoltan V. Varga, Dr. Pal Pacher
National Institute on Alcohol Abuse and Alcoholism, National Institutes of Health, Rockville, MD 20852, United States of America

[j] Prof. Dr. Cecilia J. Hillard
Department of Pharmacology and Toxicology, Neuroscience Research Center, Medical College of Wisconsin, Milwaukee, WI 53226, United States of America

[k] Dr. Peter J. McCormick
William Harvey Research Institute, Barts and the London School of Medicine, Queen Mary University of London, London EC1M 6BQ, England

[l] Dr. Zoltan Varga
HCEMM-SU Cardiometabolic Immunology Research Group, Department of Pharmacology and Pharmacotherapy, Semmelweis University, 1085 Budapest, Hungary

[m] Dr. Sergio Oddi
Faculty of Veterinary Medicine, University of Teramo, 64100 Teramo, Italy

[n] Dr. Sergio Oddi, Prof. Dr. Mauro Maccarrone
European Center for Brain Research (CERC)/Santa Lucia Foundation, 00179 Rome, Italy

[o] Prof. Dr. Mauro Maccarrone
Department of Medicine, Campus Bio-Medico University of Rome, 00128, Rome, Italy

Introduction

G protein-coupled receptors (GPCRs) are key mediators of a wide range of cell signaling processes.[1] Due to their therapeutic potential in disease modulation and their tractability as membrane proteins, GPCRs constitute one of the most important druggable human receptor families.[2] Among them, cannabinoid type 1 and type 2 receptors (CB_1R and CB_2R) are key transducers of extracellular stimuli in the endocannabinoid signaling system (eCB system), which is a fundamental lipid signaling system for all vertebrates and responsible for eliciting multiple physiological processes.[3] While CB_1R is mainly expressed in the central nervous system and only to a lesser extent in peripheral tissue, CB_2R is primarily expressed in immune cells.[4] There is growing evidence that in particular CB_2R signaling impairment is correlated with several pathologies, especially tissue injury and inflammatory conditions[5] including kidney, cardiovascular, gastrointestinal, lung, neurodegenerative and psychiatric diseases, as well as pain and cancer.[6] Despite the evident potential of CB_2R as prime drug target, the underlying receptor-ligand interactions and molecular mechanisms driving the pharmacological response remain poorly understood. In particular, tissue and cell-type specific receptor expression profiles are largely uncharted due to the lack of appropriate chemical tools. The situation is further aggravated by the absence of specific antibodies for both human and rodent CB_2R, thus preventing further investigations at a cellular or sub-cellular level.[7] In addition, CB_2R is expressed at very low levels in native cells and tissues and is known for its inducible nature.[8] Because the successful development of new drugs requires a thorough understanding of molecular and cellular mechanisms of action,[9] chemical probes targeting CB_2R are urgently needed.

While positron emission tomography (PET) tracers were recently used to explore CB_2R expression at tissue level,[10] this technique lacks the required cellular resolution.[11] In contrast, fluorescent imaging probes have emerged as high resolution tools to investigate localization, structure, dynamics and function of proteins and GPCRs in living cells.[12] In addition, such probes offer the potential for generating equilibrium and kinetic binding data in a high-throughput fashion, without handling radioactive material. Despite recent progress, no reversible high affinity probe with favorable fluorescence properties and the required specificity for CB_2R is currently available, hampering the accurate investigation of CB_2R pharmacology in live cells.[13] Major obstacles encountered for the development of such a probe are the high lipophilic nature of phytocannabinoid derived CB_2R ligands, which often served as starting points for probe generation. Together with the use of highly lipophilic dyes, this can synergistically lead to non-specific membrane binding and insufficient overall properties for reliable and general applications.[14] Furthermore, to ensure high translatability of preclinical pharmacological animal data to clinics and potentially apply a CB_2R fluorescent probe for dose selection in humans, the fluorescent probe should be devoid of interspecies

differences between rodent and human CB_2Rs. In this work, we report the design and synthesis of a selective, high affinity CB_2R-agonist fluorescent ligand toolbox and its pharmacological evaluation in *in vitro* binding and functional assays. We illustrate their application by cross-validation using flow cytometry, non-radioactive determination of equilibrium constants and binding kinetics using time-resolved fluorescence resonance energy transfer (TR-FRET) technology, as well as cellular trafficking studies in confocal live cell imaging.

Results and Discussion

For our modular design approach of the fluorescent ligand we considered three main features: (*i*) a recognition element (pharmacophore) that tolerates further chemical functionalization while preserving its affinity and selectivity towards the target, (*ii*) an appropriate fluorescent dye, and (*iii*) a linker that separates these two functionalities.[12] This allows for placement of the dye outside the receptor in the extracellular space (Figure 1). Linker attachment providing the wrong exit vector, in combination with a bulky and charged fluorescent dye – which is often larger than the recognition element itself – leads to a severe perturbation of the receptor-ligand interaction or even to a complete loss of binding affinity. Therefore, selection of the ideal linker attachment point as well as optimization of its length and composition are crucial for avoiding detrimental interactions with the receptor.[15] For the generation of our probes, we combined these considerations with a reverse design approach,[16] in order to capitalize from drug precursors with optimal affinity and drug-likeness (Supplementary table S-1). Such an approach may reduce the risk of unspecific cellular membrane interactions of phytocannabinoid derived recognition elements. We selected 2,5,6-trisubstituted pyrazine **RO6839251** (**1**)[17] and pyridine **RO6852763** (**2**)[18] which are derived from a CB_2R agonist drug discovery program as starting points for probe design (Figure 1A, and Supplementary table S-1). Both molecules possess subnanomolar affinities for the human CB_2 receptor (hCB_2R) and similar good binding affinity for mouse CB_2R (mCB_2R) with K_i values of 2 nM. Pyrazine **1** exhibits a 3'100-fold binding selectivity over hCB_1R, which is very important for visualization of low expression levels of CB_2R in the central nervous system, where CB_1R is highly expressed (CB_1R homology in the ligand-binding domain: 68%; 44% overall homology).[19] The calculated physicochemical properties of these ligands are superior to phytocannabinoid-derived molecules with regard to ALogP and polar surface area (PSA) (e.g. HU-910 ALogP: 6.7, PSA: 31.4).[20]

Fluorescent analogs of **1** and **2** were designed with the support of molecular modeling studies (Figure 1B). Parent agonists **1** and **2** possess two potential exit vectors which have been exploited for the elaboration of a robust structure-activity relationship[17-18], thereby providing a basis for linker placement at different positions. Candidate molecules were docked into the CB_2R binding cavity and prioritized on the likelihood of linker trajectory to reach

the extracellular space. This analysis suggested two different linker attachment sites: one at position 6 of the heteroaryl ring, the other at the geminal diethyl group (Figure 1A). Additionally, *in silico* docking studies indicated that a linker length ranging from 1 to 4 polyethylene glycol (PEG) units would be sufficient to reach out to the extracellular space.

Considering the highly lipophilic nature of the CB_2R binding cavity, a less polar alkyl linker was additionally selected to exclude detrimental effects by the pre-organized and highly hydrated PEG chain along the inner surface of the receptor.[21]

Introduction of an exit vector at position 6 was initially pursued using pyrazine **1** as parent structure for linker attachment (Figure 1C). Ether linkers carrying a terminal small and non-charged 4-nitrobenzofurazan (NBD) dye were introduced (Supplementary scheme S-2). Ligands were subjected to radioligand binding studies using membrane preparations of Chinese Hamster Ovary (CHO) cells overexpressing either human CB_2R or CB_1R (Supplementary table S-2). However, none of the conjugated derivatives exhibited appropriate affinity on hCB_2R.

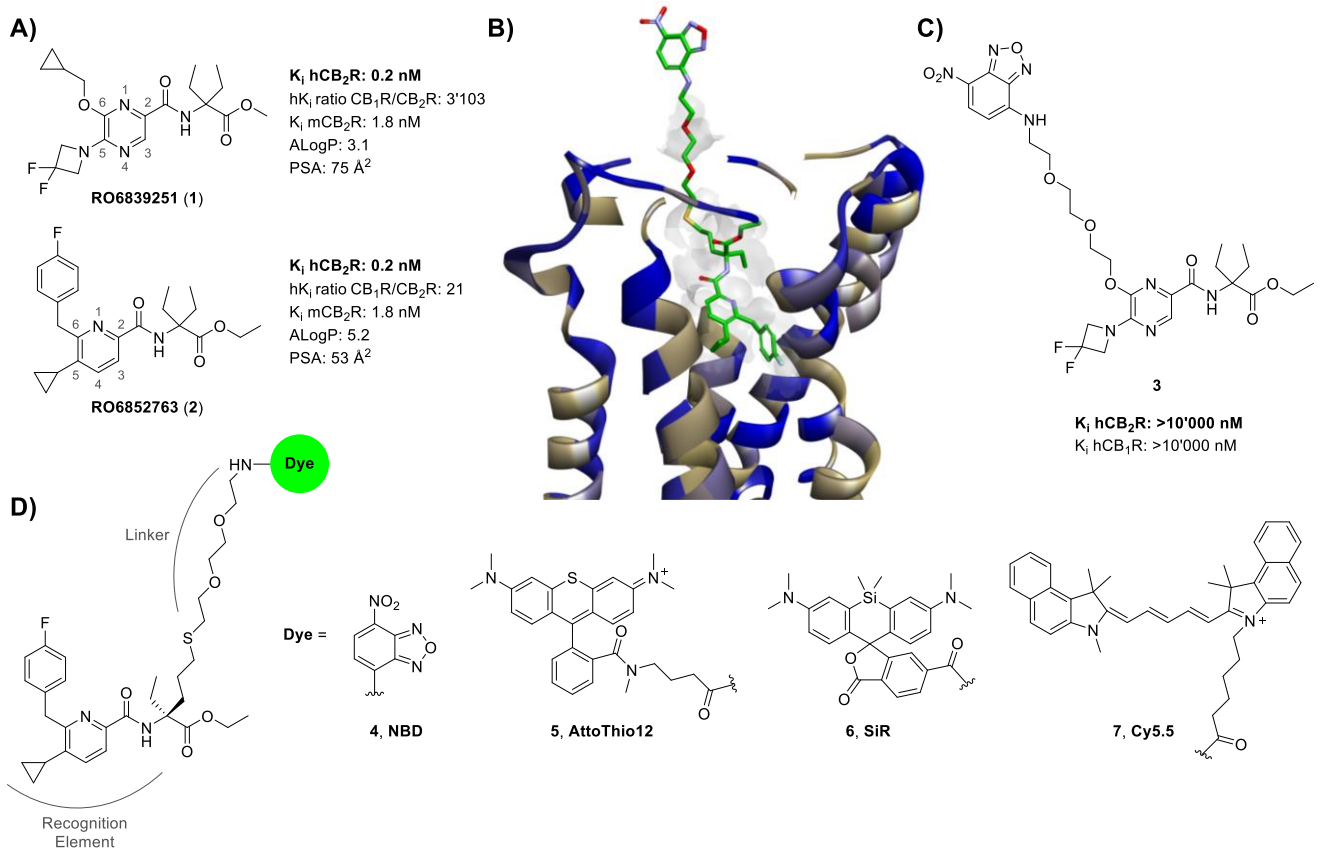

Figure 1. A) Drug discovery derived agonists **1** and **2**, used as starting points for the development of CB_2R-selective fluorescent probes; B) NBD-probe **4** docked into inactive state CB_2R X-ray structure (PDB 5ZTY);[22] Polar and hydrophobic amino acid residues are highlighted with blue and light brown colours, respectively; C) NBD-probe **3** derived from pyrazine **1** scaffold; **D)** Structure of recognition element linker construct containing a ligation handle for conjugation with NBD (**4**), AttoThio12 (**5**), SiR (**6**) and Cy5.5 (**7**) dyes. h – human, m – mouse, AlogP – calculated lipophilicity value based on the contribution of each atom to the lipophilicity, PSA – polar surface area, NBD – Nitrobenzofurazan, SiR – Silicon Rhodamine, Cy5.5 – Cyanine 5.5

Surprisingly, these molecules displayed insufficient stability in buffered aqueous media with linker elimination observed over time.[23] We therefore, turned our focus to the development of fluorescent probes which are elongated at the geminal diethyl moiety (Figure 1D). To allow for a straightforward introduction of different linkers, a modifiable ligation handle was required. Prospective SAR studies conducted to explore the tolerance of the putative new conjugation site within pyrazine **1** and pyridine **2** parent structures (Supplementary tables S-3 and S-4) indicated that elongating with a thioether would be most successful at retaining high CB_2R affinity, as seen e.g. for **SI-35** (hCB_2R K_i of 1.3 nM; Supplementary table S-4). Despite their structural similarity, pyridine **2** analogs surprisingly exhibited higher affinity for CB_2R compared to their corresponding pyrazine **1** derived congeners (Supplementary tables S-3 and S-4). Consequently, we focused our synthetic efforts on the pyridine scaffold. The preparation of **(*S*)-17** as precursor platform for the attachment of fluorescent dyes commenced with the synthesis of recognition element **11** and linker building block **(*S*)-16** (Scheme 1). Carboxylic acid **11** was prepared in 5 steps with an overall yield of 12%, starting from commercially available 3-bromo-2-methylpyridine **8**. Linker template **(*S*)-16** was synthesized starting from aminobutyric acid **12**, which was converted to olefin **13** in 4 steps using a modified literature procedure.[24] Subsequent Fmoc protection was performed to allow for separation of enantiomers by preparative chiral HPLC (see Supplementary Information (SI) for details). Hydroboration of Fmoc-protected **(*S*)-14**, followed by thio-Mitsunobu reaction afforded **(*S*)-15**. The concomitant introduction of the desired linker chain and its amine deprotection under basic conditions provided **(*S*)-16**. Subsequent amide coupling of **(*S*)-16** with acid **11** using HATU and consecutive removal of the Boc protecting group led to the final assembly step of the respective fluorescent probes **4** (NBD), **5** (AttoThio12), **6** (Silicon Rhodamine, SiR) and **7** (Cyanine 5.5, Cy5.5), as shown in Figure 1D.

For systematic investigation of the optimal linker length, racemic NBD-labeled probes containing different linker lengths ranging from PEG1 to PEG4, as well as a C6 alkyl chain were synthesized using a similar route. Subsequent evaluation of linker length indicated NBD constructs with PEG2 linker units as the most favorable with regard to CB_2R affinity (Supplementary table S-5) and was therefore used for introduction of other fluorophores with more favorable photophysical properties.

The linker attachment at one arm of the geminal diethyl moiety generated a quaternary chiral center at the α-carbon of the amino acid ester residue. To investigate the influence of stereochemistry on compound affinity and activity, enantiomer pairs of NBD-labeled probe **4** and precursor **17** were analyzed (Table 1, see also Supplementary table S-6). A comparison of precursor **17** binding data indicated that there was sufficient space around the quaternary carbon junction within the binding cavity for accommodating both stereoisomers (cf. **(*S*)-17**

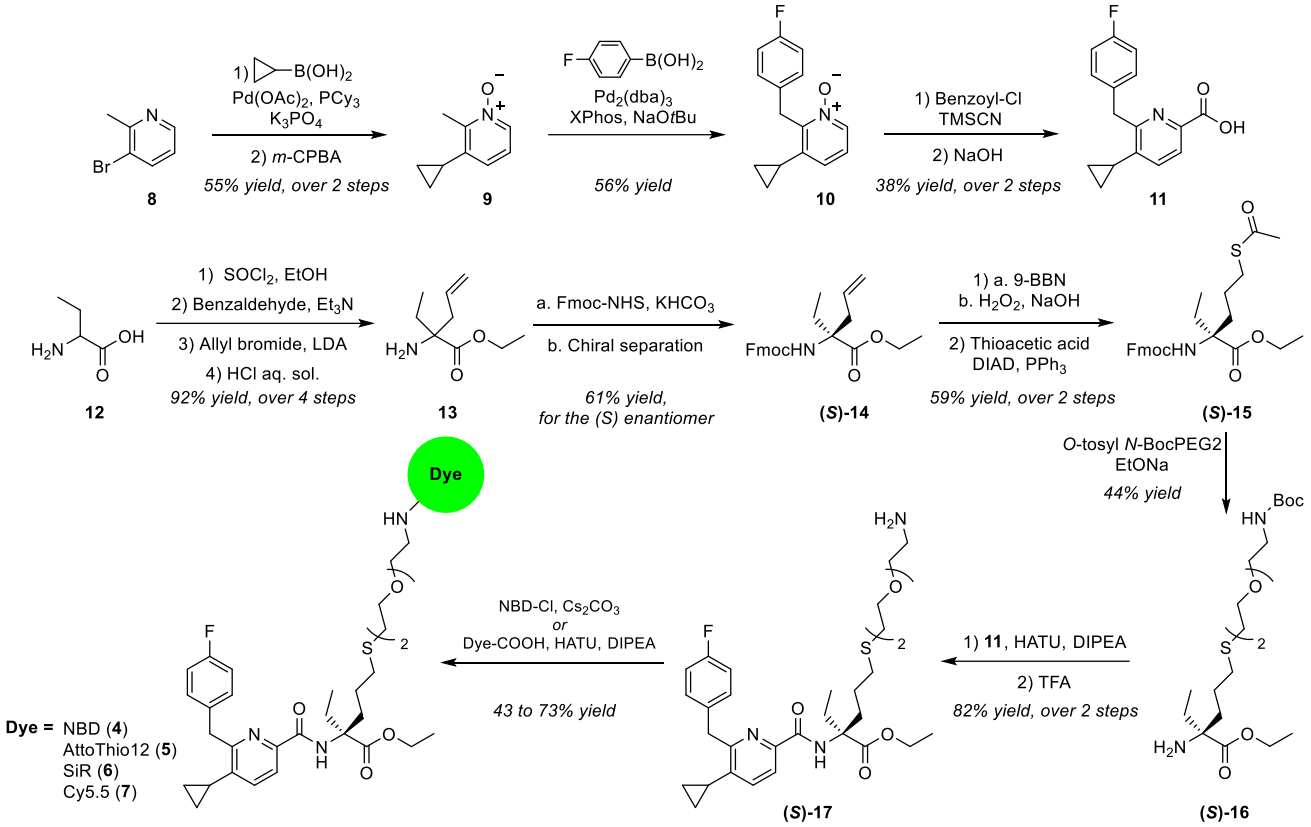

Scheme 1. General synthetic approach to CB_2R-selective fluorescently labeled probes. For synthesis details see SI

hCB_2R K_i: 2.7 nM vs. **(*R*)-17** hCB_2R K_i: 4.6 nM; Table 1, entries 2 – 3). Remarkably, a 18-fold enantio-discrimination with regard to hCB_2R binding affinity favoring the (*S*) enantiomer was observed for the fully labeled probe pair **4** (cf. **(*S*)-4** hCB2R K_i: 9.1 nM vs. **(*R*)-4** hCB2R K_i: 159 nM; Table 1, entries 4–5). A similar observation was made for mouse CB_2R, where binding of **(*S*)-4** was more pronounced with a 19-fold difference (cf. **(*S*)-4** mCB_2R K_i: 33 nM vs. **(*R*)-4** mCB_2R K_i: 622 nM; Table 1, entries 4–5). We therefore used (*S*)-configured amine **17** for introducing additional fluorescent dyes tailored toward subsequent biological investigations i.e. AttoThio12 (**5**), SiR (**6**) and Cy5.5 (**7**) (Scheme 1 and Table 1). Moreover, high potency, selectivity and agonistic properties of the probe were preserved despite linker elongation and were largely independent of dye attachment. To the best of our knowledge, these CB_2R-selective fluorescent probes are the first to preserve interspecies affinity and efficacy for both, mouse and human CB_2R. For example, AttoThio12 probe **5** (hCB_2R K_i: 3.2 nM, mCB_2R K_i: 4.6 nM, Table 1, entry 6) exhibits single digit nanomolar binding affinities on both human and mouse CB_2R. Binding selectivity versus hCB_1R was highest for **(*S*)-4** (hK_i ratio CB_1R/CB_2R: 68 Table 1, entry 4) which fully translates in functional selectivity in forskolin-stimulated cAMP release assays alongside with low nanomolar potency and full agonistic effects at CB_2R. Likewise, NBD probe **(*S*)-4** and SiR-**6** outperformed with regard to functional selectivity versus CB_1R (hEC_{50} ratio CB_1R/CB_2R for **(*S*)-4**: >4'545 and for **6**: >149, Table 1, entries 4 and 7, respectively). The ligands span a broad lipophilicity range of AlogP values from 4.5 for amine **17** through 6.3 for NBD labeled agonist **4** up to 13.7 for Cy5.5 probe **7**

indicating a significant influence of the reporter group on the overall physicochemical properties of the ligands. This was further confirmed by measuring effective permeation coefficients of pyridine **2** linker dye adducts in the parallel artificial membrane permeability assay (PAMPA). Here all NBD labeled probes were able to passively permeate through membranes (**SI-47**: P_{eff} 0.7 cm/s*10^{-6}, **SI-48**: P_{eff} 0.7 cm/s*10^{-6} and **SI-49**: P_{eff} 0.5 cm/s*10^{-6}; Supplementary table S-5), thereby suggesting that more lipophilic SiR- and Cy5.5-bearing probes **6** and **7**, respectively, are likely to be cell permeable as well.[25]

Table 1. Key characteristics of pyridine **2**, labeling precursors and fluorescent probes. Calculated lipophilicity (AlogP), binding affinity (K_i), cAMP potency and efficacy (EC_{50} (%eff.)), and absorption and emission ranges of fluorescent probes (Abs/Ems).

Entry	Compound	Dye	AlogP [a]	K_i [nM][f]			hK$_i$ ratio CB$_1$R/ CB$_2$R	cAMP EC_{50} [nM] (%Eff.)[b, f]			hEC$_{50}$ ratio CB$_1$R/ CB$_2$R	Abs/Ems [nm]
				hCB$_2$R	hCB$_1$R	mCB$_2$R		hCB$_2$R	hCB$_1$R	mCB$_2$R		
1	**2**	n.a.	5.2	0.2	5.4	1.8	27	0.7 (102)	4.4 (99)	1.9 (99)	6.3	n.a.
2	***(S)*-17**	n.a. (NH_2)	4.5	2.7	64	2.6	23	0.5 (91)	57 (84)	3.2 (91)	114	n.a.
3	***(R)*-17**	n.a. (NH_2)	4.5	4.6	180	13	39	11 (81)	>10'000	424 (61)	>909	n.a.
4	***(S)*-4**	NBD	6.3	9.1	617	33	68	2.2 (72)	>10'000	21 (95)	>4'545	474/550[c]
5	***(R)*-4**	NBD	6.3	159	4'925	622	31	17 (84)	>10'000	1'093 (69)	>588	474/550[c]
6	***(S)*-5**	AttoThio 12	9.0	3.2	63	4.6	20	n.d.	n.d.	n.d.	n.d.	582/610[c]
7	***(S)*-6**	SiR	10.6	62	114	117	2	67 (96)	>10'000	66 (93)	>149	652/674[d]
8	***(S)*-7**	Cy5.5	13.7	14	108	50	8	140 (110)	726 (118)	512 (119)	5	690/730[e]

h – human; m – mouse; n.a. – not applicable; n.d. – not determined. [a] The AlogP is a calculated value based on the contribution of each atom to the lipophilicity; [b] Functional potency (EC_{50}), percentage efficacy given in parenthesis; [c] Fluorescence excitation and emission measured in aqueous solution (DPBS, Dulbecco's phosphate buffered saline); [d] Fluorescence excitation and emission derived from literature;[25] [e] Fluorescence excitation and emission measured in DMSO; [f] Assay description and reference ligands data described in the SI.

With this set of highly potent and selective CB_2R fluorescent probes in hand we aimed to further illustrate the usefulness of this toolbox through validation studies in an array of more complex chemical biology investigations. The novel probes were subjected to FACS studies, they were utilized for kinetic and equilibrium binding studies via time-resolved fluorescence resonance energy transfer (TR-FRET) assays, and exploited for confocal time-lapse imaging. Thereby, we could demonstrate for the first time displacement of CB_2R reference ligands in flow cytometry experiments, generation of CB_2R kinetic and equilibrium binding data applying fluorescence based techniques and visualization of CB_2R trafficking and internalization in living cells.

To study the specificity of our novel fluorescently labeled probes for human and mouse CB_2R, CHO cells overexpressing either hCB_2R, mCB_2R or hCB_1R as well as control WT-CHO cells were incubated with different concentrations of AttoThio12-labeled **5** (Figure 2A) and SiR-labeled **6** probes (Figure 2B). In comparison to hCB_1R overexpressing cells or WT-CHO cells, probes **5** and **6** were highly specific for CHO cells overexpressing either hCB_2R or mCB_2R. Probes **5** and **6** showed a significant concentration-dependent increase in mean fluorescence

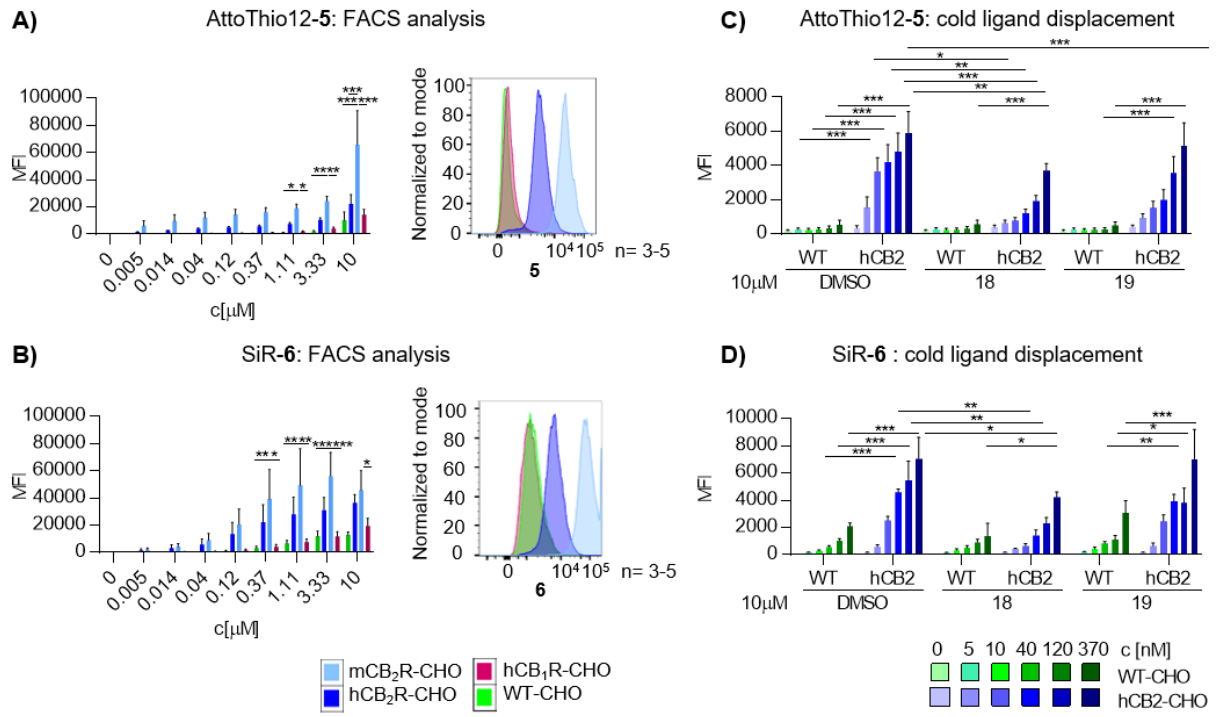

Figure 2. A, B) FACS analysis of the mean fluorescent intensity (MFI) of WT, hCB_2R, mCB_2R and hCB_1R overexpressing CHO cells incubated with different concentration of **5** or **6**. FACS plots show representative histograms of cells incubated with 0.37 µM ligand; C, D) FACS analysis of WT and hCB_2R -CHO cells pretreated with **18** or **19** (10 µM) and stained with different concentrations of **5** or **6** (*right panels*). Mean ± SEM. Two-way- ANOVA, * p<0.05; ** p<0.01; *** p< 0.005.

intensity for concentrations ranging from 0.4 µM to 3.3 µM for **5** and 1.1 µM to 10 µM for **6**. To further confirm ligand specificity and exclude unspecific binding, we investigated whether these fluorescent compounds can compete for the CB_2R binding site with the known cold CB_2R ligands, agonist JWH133 (**18**),[20] and inverse agonist RO6851228 (**19**)[26] (Figure 2C and 2D). After pre-incubation of WT-CHO or hCB_2R-CHO cells with ligands **18** and **19**, AttoThio12-**5** and SiR-**6** could both efficiently displace CB_2R-agonist **18** at a broad concentration range. Moreover, 0.37 µM **5** or **6** also displaced inverse agonist **19** illustrating the high degree of target specificity of the fluoroprobes AttoThio12-**5** and SiR-**6** in a cellular setting.

Up to now the generation of CB_2R equilibrium and kinetic binding data has been exclusively based on tritiated CB_2R ligands, precluding it from standard high-throughput screening.[27] Time-resolved fluorescence resonance energy transfer (TR-FRET) offers an attractive alternative for obtaining such data, thereby avoiding radiometric assays.[28] Using this technique, we measured the binding kinetics of our CB_2R-specific probes AttoThio12-**5**, SiR-**6** and Cy5.5-**7**, alongside the affinity of the CB_2R specific ligands, agonist HU-308 (**20**),[20, 29] and inverse agonist SR144528 (**21**).[20, 30] Binding kinetics of probes **6** and **7** was characterized by monitoring the observed association rates (k_{obs}, min^{-1}) at different ligand concentrations (Figure 3A, and Supplementary figure S-3A). The observed rate of fluorescent ligand association (k_{obs}) was related to CB_2R fluorescent ligand concentration in a linear fashion

(Figure 3A, *right panel*, and Supplementary figure S-3B). Kinetic rate parameters k_{off} (min^{-1}) and k_{on} ($M^{-1}min^{-1}$) were calculated by globally fitting association time courses. The resulting K_d (k_{off} / k_{on}) values were in very good agreement to those obtained from the equilibrium studies and those determined indirectly through radioligand binding studies (Figure 3B, and Supplementary figure S-3C). The binding affinity of probe **5** was determined through equilibrium saturation binding (Supplementary table S-10, saturation K_d of **5** is 19 nM). To confirm the applicability of fluorescent ligands **6** and **7** as tracers, the binding affinity of CB_2R ligands **20** and **21** were determined (Figure 3C, and Supplementary figure S-4 and table S-11). Overall, comparing our TR-FRET data with the values obtained from radioligand binding assays, we found excellent agreement with our own and previously published data for the CB_2R ligands tested.[20, 29-30] These results illustrate the potential of implementing TR-FRET methodology for CB_2R ligand residence time investigation and for application in high-throughput screening.

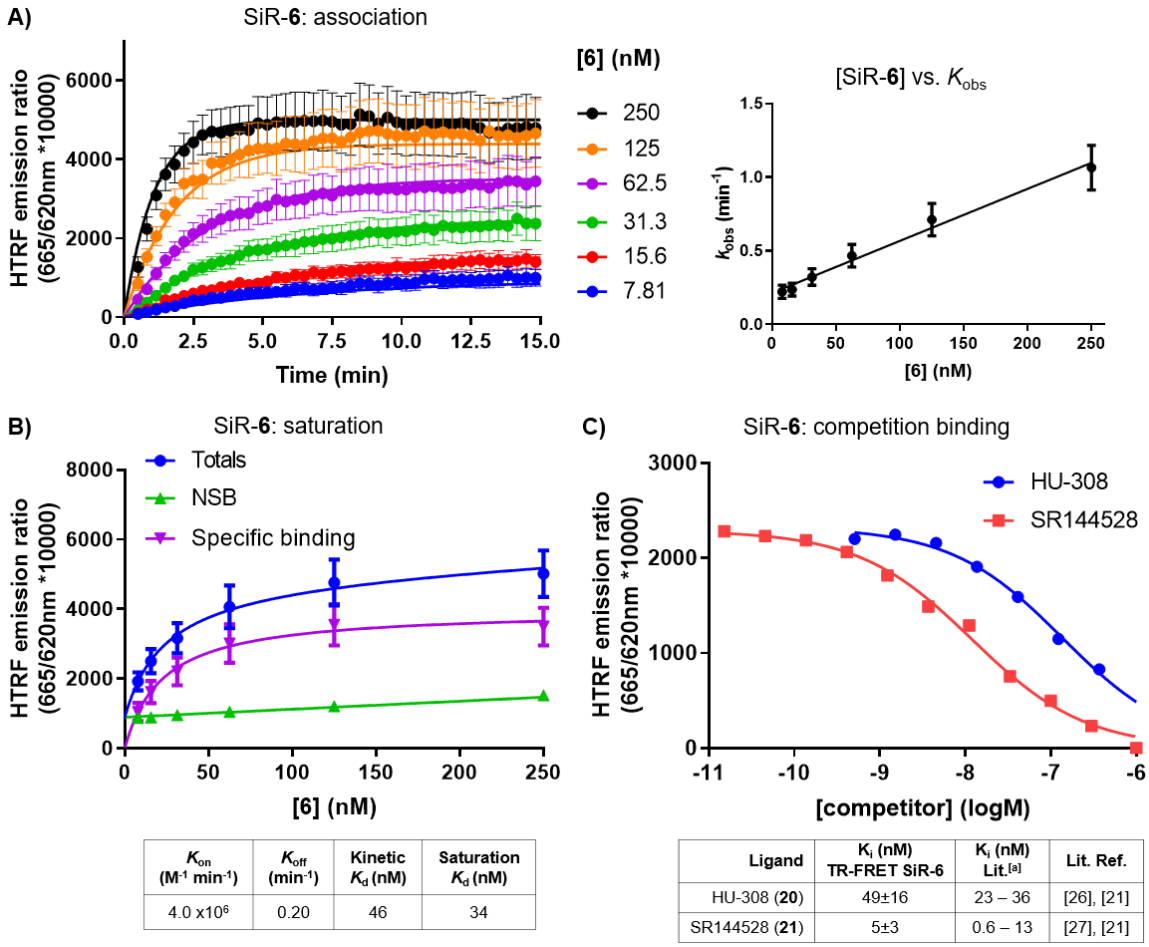

K_{on} (M^{-1} min^{-1})	K_{off} (min^{-1})	Kinetic K_d (nM)	Saturation K_d (nM)
4.0 x10^6	0.20	46	34

Ligand	K_i (nM) TR-FRET SiR-6	K_i (nM) Lit.[a]	Lit. Ref.
HU-308 (**20**)	49±16	23 – 36	[26], [21]
SR144528 (**21**)	5±3	0.6 – 13	[27], [21]

Figure 3. HTRF-based characterization of SiR-**6** with determination of kinetic and equilibrium binding parameters using HEK-hCB_2R cell membranes: A) Observed association of **6** binding to hCB_2R (*left panel*), and plot of **6** concentration vs. k_{obs} (*right panel*); B) Saturation analysis showing binding of **6** to hCB_2R. Kinetic and equilibrium data were used to calculate K_d, and k_{on} and k_{off} values for fluorescent ligands (*lower panel*); C) Competition binding studies between **6** and increasing concentrations of CB_2R specific ligands **20** (HU-308) and **21** (SR144528) for hCB_2R. Data were used to calculate K_i values for **20** and **21** (*lower panel*) with literature data shown for comparison (**20** K_i: 23 nM[29] and 36 nM;[20] **21** K_i: 0.6 nM[30] and 13 nM[20]). [a]Literature data obtained from radioligand binding assay

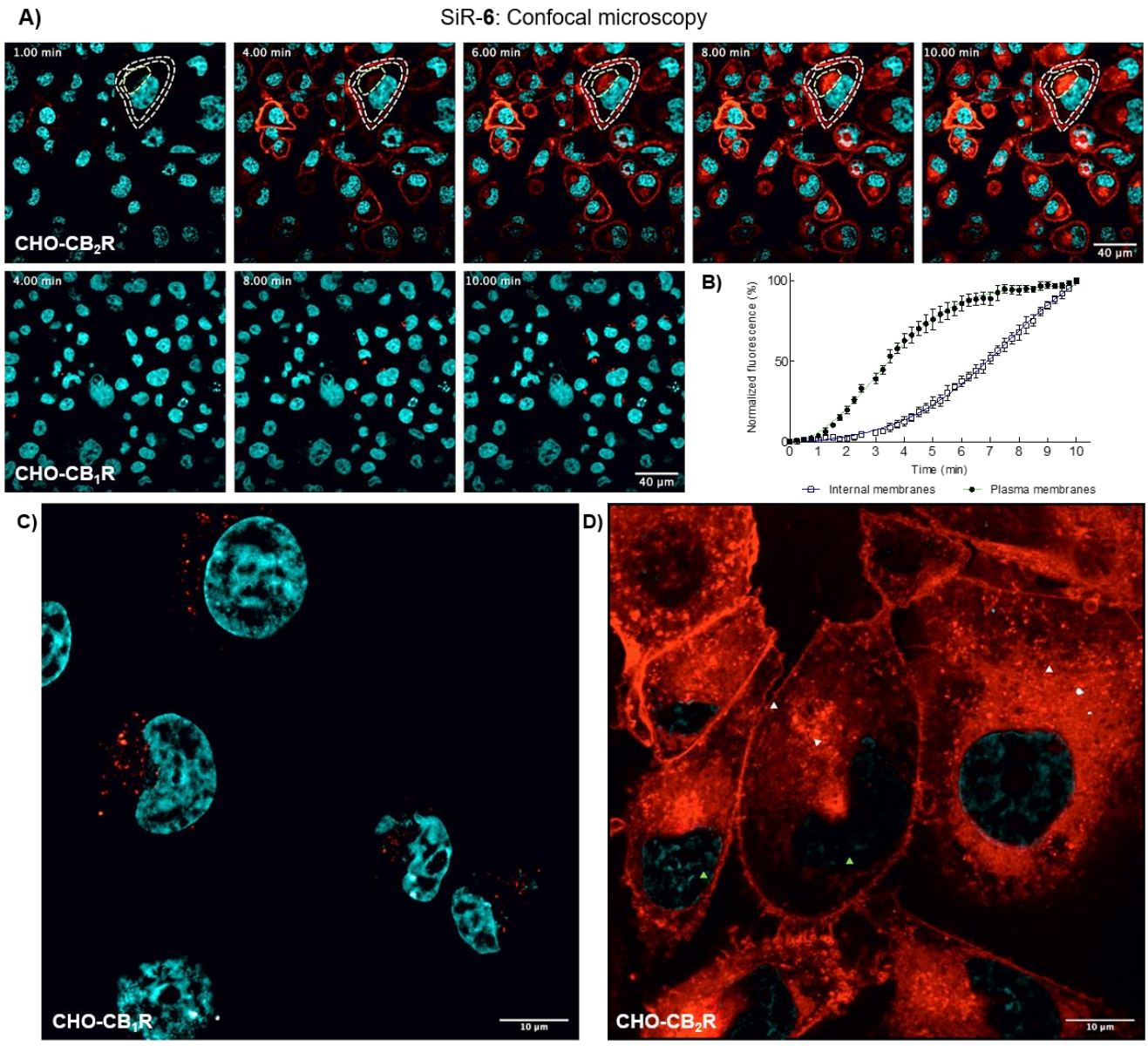

Figure 4. A) Time-lapse confocal microscopy frames for hCB_2R (*upper panels*) and hCB_1R (*lower panels*). CHO cells co-stained with **6** (red) and Hoechst 33342 (cyan, nucleus counter stain) at 1, 4, 6, 8 and 10 min; Plasma and internal membranes are highlighted with white and yellow dashes, respectively; B) Association curve of 0.4 µM **6** on plasma membrane and internal membranes of hCB_2R-CHO cells; (C, D) Airyscan high-resolution imaging of hCB_1R- and hCB_2R-overexpressing CHO cells incubated either for 10 min with 0.4 µM **6** (red) and counterstained with Hoechst 33342 (cyan). C) hCB_1R cells displayed only negligible staining resulting as sparse dot structures near to the cell nucleus; D) In hCB_2R cells, **6** was readily incorporated into plasma membranes, and reached nearly all internal membranes within 10 minutes, particularly those located in the perinuclear zone, resembling endoplasmic reticulum and/or Golgi complex (green triangles). Small vesicles, reminiscent of early endosomes (white triangles), appeared below the plasma membrane and within the cytosol

The suitability of SiR-**6** to specifically visualize hCB_2R in living cells was subsequently evaluated by confocal time-lapse imaging. Exposure of hCB_2R-overexpressing CHO cells with **6** resulted in a clear labeling of cell membranes, which was time- and concentration dependent. Plasma membrane labeling with 0.4 µM **6** was detectable within 3 min and increased progressively over time, reaching a steady-state plateau after 6 min and remained unchanged up to 10 min (Figure 4A, *upper panels*, and 4B). In accordance with the results obtained for the NBD-labeled analogues in the PAMPA assay (Supplementary table S-5) probe SiR-**6** is a membrane-permeable

ligand and was able to successively enter hCB_2R-overexpressing cells and reach nearly all internal membranes (Figure 4A and D). The kinetic analysis of the fluorescence signal measured on the CB_2R-containing internal membranes showed that loading of **6** did not reach saturation after 10 minutes (Figure 4B). Image acquisition at higher magnification and resolution shows that, besides the cell membrane, labeled hCB_2R was detected in intracellular compartments, predominantly within perinuclear structures, reminiscent of Golgi complex and endoplasmic reticulum (Figure 4D, *green and white triangles, respectively*). During the time-course of staining, small endosome-like vesicles (Figure 4D, *white triangles*) appeared just below the plasma membrane and within the cytosol, suggesting the presence of an agonist-stimulated internalization process of the CB_2R, along with passive diffusion of the probe. Moreover, SiR probe-**6** was nearly non-fluorescent in aqueous environments, allowing bright labeling of cellular membranes even in the continued presence of the probe in the culture medium, thus permitting experimental imaging studies over prolonged time (Figure 4A, *lower panels*, and 4C). Importantly, in control CB_1R-overexpressing CHO cells, **6** did not produce membrane labeling under these conditions, demonstrating the high CB_2R-specificity and remarkably low extent of unspecific binding of this fluoroprobe (Figure 4A, *lower panels*). All together, these results show that cell permeable SiR probe-**6** allows accurate tracing of CB_2R receptor subcellular distribution and trafficking dynamics, as well as staining its total cellular content in real-time live cell imaging.

Conclusion

Following a reverse design approach, a toolbox of highly potent and CB_2R-specific fluorescent probes was developed and cross-validated in different experimental settings conducted in multiple laboratories. Assisted by molecular modeling studies, preclinical CB_2R agonist drug **2** was advanced into a CB_2R probe precursor platform **(*S*)-17**, which allowed the attachment of a variety of dyes with different physicochemical and photophysical properties tailored for diverse applications. Despite large structural modifications with regard to linker elongation and dye attachment, high potency, selectivity and agonistic properties of the parent drug were mostly preserved. To the best of our knowledge, these CB_2R-selective fluorescent probes are the first to show highly consistent interspecies affinity and efficacy for both human and mouse CB_2R in the nanomolar range. In flow cytometry experiments (AttoThio12-**5** and SiR-**6**), we could specifically label CB_2R overexpressing cells and demonstrate target specificity by competition against CB_2R reference ligands. In a novel fluorescence based TR-FRET assay, probes (SiR-**6** and Cy5.5-**7**) allowed generation of CB_2R kinetic and equilibrium binding data, which were in excellent agreement with previous values obtained using radiometric ligand-binding assays. In addition, fluoroprobe

SiR-**6** was employed to reliably image and monitor CB_2R distribution in real-time live cell imaging by confocal microscopy.

We believe that our novel CB_2R fluorescent probes may help to elucidate CB_2R molecular and cellular mechanism of action, as well as to unravel its expression levels in different tissues and disease states. Therefore, this toolbox holds great potential to complement present knowledge on CB_2R pharmacology.

Acknowledgements

MN, TG, BB, MW and YM would like to thank Dr. Edgar Specker, Sandra Miksche and the NMR core facility of the FMP for their excellent support on compound characterization. We are grateful to Dr. Barth van Rossum for preparing graphical artwork. We greatly acknowledge the chiral separation of key building block **SI-59** by Daniel Zimmerli and Erik Hunziker. Some aspects of developing TR-FRET assay were supported by the Swiss National Science Foundation grant 159748 to DBV. MM and SO thank Dr. Lucia Scipioni and Dr. Antonio Totaro for cell culture and technical support, and Dr. Daunia Laurenti for her technical assistance in live imaging. They are also grateful to the Italian Ministry of Education, University and Research (MIUR) for partial financial support under the competitive grant PRIN 2015. The determination of solubility data by Catherine Karrer and logD values by Aynur Ekiciler is greatly acknowledged. We furthermore thank Björn Wagner, Virginie Micallef and Joelle Muller for the generation of PAMPA data. We thank Prof. Dr. Mathias Christmann, Prof. Dr. Rainer Haag and PD Dr. Daniel Häussinger for helpful discussions. This work was partially supported by the Sino-German research project grant (GZ 1271) to MN.

Keywords: fluorescent probe • cannabinoid type 2 receptor (CB_2R) • reverse design • toolbox • live cell imaging

[1] R. Sridharan, J. Zuber, S. M. Connelly, E. Mathew, M. E. Dumont, *Biochim. Biophys. Acta* **2014**, *1838*, 15-33.

[2] J. P. Overington, B. Al-Lazikani, A. L. Hopkins, *Nat. Rev. Drug Discov.* **2006**, *5*, 993-996.

[3] a) S. Munro, K. L. Thomas, M. Abu-Shaar, *Nature* **1993**, *365*, 61-65; b) W. A. Devane, F. A. Dysarz, M. R. Johnson, L. S. Melvin, A. C. Howlett, *Mol. Pharmacol.* **1988**, *34*, 605-613.

[4] a) C. Turcotte, M.-R. Blanchet, M. Laviolette, N. Flamand, *Cell. Mol. Life Sci.* **2016**, *73*, 4449-4470; b) S. Galiegue, S. Mary, J. Marchand, D. Dussossoy, D. Carriere, P. Carayon, M. Bouaboula, D. Shire, G. Le Fur, P. Casellas, *Eur. J. Biochem.* **1995**, *232*, 54-61.

[5] a) P. Pacher, R. Mechoulam, *Prog. Lipid Res.* **2011**, *50*, 193-211; b) J. Guindon, A. G. Hohmann, *Br. J. Pharmacol.* **2008**, *153*, 319-334.

[6] a) R. P. Picone, D. A. Kendall, *Mol. Endocrinol.* **2015**, *29*, 801-813; b) A. M. Malfitano, S. Basu, K. Maresz, M. Bifulco, B. N. Dittel, *Semin. Immunol.* **2014**, *26*, 369-379; c) R. G. Pertwee, *Philos. Trans. R. Soc.* **2012**, *367*, 3353-3363.

[7] a) H. Y. Zhang, H. Shen, C. J. Jordan, Q. R. Liu, E. L. Gardner, A. Bonci, Z. X. Xi, *Acta Pharmacol. Sin.* **2019**, *40*, 398-409; b) B. Cécyre, S. Thomas, M. Ptito, C. Casanova, J.-F. Bouchard, *Naunyn-*

Schmiedeberg's Arch. Pharmacol. **2014**, *387*, 175-184; c) Y. Marchalant, P. W. Brownjohn, A. Bonnet, T. Kleffmann, J. C. Ashton, *J. Histochem. Cytochem.* **2014**, *62*, 395-404.

[8] a) A. Cooper, S. Singh, S. Hook, J. D. A. Tyndall, A. J. Vernall, *Pharmacol. Rev.* **2017**, *69*, 316-353; b) N. L. Grimsey, C. E. Goodfellow, M. Dragunow, M. Glass, *Biochim. Biophys. Acta* **2011**, *1813*, 1554-1560.

[9] a) D. S. Tyler, J. Vappiani, T. Caneque, E. Y. N. Lam, A. Ward, O. Gilan, Y. C. Chan, A. Hienzsch, A. Rutkowska, T. Werner, A. J. Wagner, D. Lugo, R. Gregory, C. Ramirez Molina, N. Garton, C. R. Wellaway, S. Jackson, L. MacPherson, M. Figueiredo, S. Stolzenburg, C. C. Bell, C. House, S. J. Dawson, E. D. Hawkins, G. Drewes, R. K. Prinjha, R. Rodriguez, P. Grandi, M. A. Dawson, *Science* **2017**, *356*, 1397-1401; b) G. M. Simon, M. J. Niphakis, B. F. Cravatt, *Nat. Chem. Biol.* **2013**, *9*, 200-205.

[10] R. Slavik, U. Grether, A. Müller Herde, L. Gobbi, J. Fingerle, C. Ullmer, S. D. Krämer, R. Schibli, L. Mu, S. M. Ametamey, *J. Med. Chem.* **2015**, *58*, 4266-4277.

[11] A. R. Kherlopian, T. Song, Q. Duan, M. A. Neimark, M. J. Po, J. K. Gohagan, A. F. Laine, *BMC Syst Biol* **2008**, *2*, 74-92.

[12] L. A. Stoddart, L. E. Kilpatrick, S. J. Briddon, S. J. Hill, *Neuropharmacology* **2015**, *98*, 48-57.

[13] a) S. Singh, C. R. M. Oyagawa, C. Macdonald, N. L. Grimsey, M. Glass, A. J. Vernall, *ACS Med. Chem. Lett.* **2019**, *10*, 209-214; b) M. Soethoudt, S. C. Stolze, M. V. Westphal, L. van Stralen, A. Martella, E. J. van Rooden, W. Guba, Z. V. Varga, H. Deng, S. I. van Kasteren, U. Grether, A. P. IJzerman, P. Pacher, E. M. Carreira, H. S. Overkleeft, A. Ioan-Facsinay, L. H. Heitman, M. van der Stelt, *J. Am. Chem. Soc.* **2018**, *140*, 6067-6075; c) X. Ling, S. Zhang, P. Shao, W. Li, L. Yang, Y. Ding, C. Xu, N. Stella, M. Bai, *Biomaterials* **2015**, *57*, 169-178; d) S. Zhang, P. Shao, M. Bai, *Bioconjug. Chem.* **2013**, *24*, 1907-1916; e) L. Martín-Couce, M. Martín-Fontecha, Ó. Palomares, L. Mestre, A. Cordomí, M. Hernangomez, S. Palma, L. Pardo, C. Guaza, M. L. López-Rodríguez, S. Ortega-Gutiérrez, *Angew. Chem. Int. Ed.* **2012**, *51*, 6896-6899; f) R. R. Petrov, M. E. Ferrini, Z. Jaffar, C. M. Thompson, K. Roberts, P. Diaz, *Bioorg. Med. Chem. Lett.* **2011**, *21*, 5859-5862; g) M. Sexton, G. Woodruff, E. A. Horne, Y. H. Lin, G. G. Muccioli, M. Bai, E. Stern, D. J. Bornhop, N. Stella, *Chem. Biol.* **2011**, *18*, 563-568.

[14] A. J. Vernall, S. J. Hill, B. Kellam, *Br. J. Pharmacol.* **2014**, *171*, 1073-1084.

[15] K. A. Jacobson, *Bioconjug. Chem.* **2009**, *20*, 1816-1835.

[16] A. Watzke, G. Kosec, M. Kindermann, V. Jeske, H. P. Nestler, V. Turk, B. Turk, K. U. Wendt, *Angew. Chem. Int. Ed.* **2008**, *47*, 406-409.

[17] B. Dhurwasulu, U. Grether, M. Nettekoven, S. Roever, M. Rogers-Evans, T. Schulz-Gasch (F. H.-L. Roche), WO2014086807A1, **2014**.

[18] C. Bissantz, U. Grether, P. Hebeisen, A. Kimbara, Q. Liu, M. Nettekoven, M. Prunotto, S. Roever, M. Rogers-Evans, T. Schulz-Gasch, C. Ullmer, Z. Wang, W. Yang (F. H.-L. Roche), WO2012168350A1, **2012**.

[19] a) K. Mackie, *Handb. Exp. Pharmacol.* **2005**, 299-325; b) S. Munro, K. L. Thomas, M. Abu-Shaar, *Nature* **1993**, *365*, 61-65.

[20] M. Soethoudt, U. Grether, J. Fingerle, T. W. Grim, F. Fezza, L. de Petrocellis, C. Ullmer, B. Rothenhäusler, C. Perret, N. van Gils, D. Finlay, C. MacDonald, A. Chicca, M. D. Gens, J. Stuart, H. de Vries, N. Mastrangelo, L. Xia, G. Alachouzos, M. P. Baggelaar, A. Martella, E. D. Mock, H. Deng, L. H. Heitman, M. Connor, V. Di Marzo, J. Gertsch, A. H. Lichtman, M. Maccarrone, P. Pacher, M. Glass, M. van der Stelt, *Nat. Commun.* **2017**, *8*, 13958.

[21] A. J. Vernall, S. J. Hill, B. Kellam, *Brit. J. Pharmacol.* **2014**, *171*, 1073-1084.

[22] X. Li, T. Hua, K. Vemuri, J.-H. Ho, Y. Wu, L. Wu, P. Popov, O. Benchama, N. Zvonok, K. a. Locke, L. Qu, G. W. Han, M. R. Iyer, R. Cinar, N. J. Coffey, J. Wang, M. Wu, V. Katritch, S. Zhao, G. Kunos, L. M. Bohn, A. Makriyannis, R. C. Stevens, Z.-J. Liu, *Cell* **2019**, *176*, 459-467.

[23] S. P. Mcmanus, R. M. Karaman, M. R. Sedaghat-Herati, T. G. Shannon, T. W. Hovatter, J. M. Harris, *J. Polym. Sci., Part A: Polym. Chem.* **1990**, *28*, 3337-3346.

[24] W. Liu, P. Ray, S. A. Benezra, *J. Chem. Soc., Perkin Trans. 1* **1995**, 553-559.

[25] G. Lukinavicius, K. Umezawa, N. Olivier, A. Honigmann, G. Yang, T. Plass, V. Mueller, L. Reymond, I. R. Correa, Jr., Z. G. Luo, C. Schultz, E. A. Lemke, P. Heppenstall, C. Eggeling, S. Manley, K. Johnsson, *Nat. Chem.* **2013**, *5*, 132-139.

[26] N. Ouali Alami, C. Schurr, F. Olde Heuvel, L. Tang, Q. Li, A. Tasdogan, A. Kimbara, M. Nettekoven, G. Ottaviani, C. Raposo, S. Röver, M. Rogers-Evans, B. Rothenhäusler, C. Ullmer, J. Fingerle, U. Grether, I. Knuesel, T. M. Boeckers, A. Ludolph, T. Wirth, F. Roselli, B. Baumann, *EMBO J.* **2018**, *37*, e98697.

[27] A. Martella, H. Sijben, A. Rufer, J. Fingerle, U. Grether, C. Ullmer, T. Hartung, A. IJzerman, M. van der Stelt, L. Heitman, *Mol. Pharmacol.* **2017**, *92*, 389-400.

[28] L. Chen, L. Jin, N. Zhou, *Expert Opin. Drug Discov.* **2012**, *7*, 791-806.

[29] L. Hanuš, A. Breuer, S. Tchilibon, S. Shiloah, D. Goldenberg, M. Horowitz, R. G. Pertwee, R. A. Ross, R. Mechoulam, E. Fride, *PNAS* **1999**, *96*, 14228-14233.

[30] M. Rinaldi-Carmona, F. Barth, J. Millan, J. M. Derocq, P. Casellas, C. Congy, D. Oustric, M. Sarran, M. Bouaboula, B. Calandra, M. Portier, D. Shire, J. C. Breliere, G. L. Le Fur, *J. Pharmacol. Exp. Ther.* **1998**, *284*, 644-650.